Unambiguous identification of N-containing oxygenated organic molecules using CI-Orbitrap in an eastern Chinese megacity

Yiqun Lu[1,2], Yingge Ma[1], Dan Dan Huang[1], Shengrong Lou[1], Sheng'ao Jing[1], Yaqin Gao[1], Hongli Wang[1], Yanjun Zhang[3], Hui Chen[4], Yunhua Chang[5], Naiqiang Yan[2], Jianmin Chen[4], Christian George[3], Matthieu Riva[3], Cheng Huang[1]*

[1] State Environmental Protection Key Laboratory of Formation and Prevention of Urban Air Pollution Complex, Shanghai Academy of Environmental Sciences, Shanghai 200233, China;

[2] School of Environmental Science and Engineering, Shanghai Jiao Tong University, Shanghai 200240, China

[3] Univ. Lyon, Université Claude Bernard Lyon1, CNRS, IRCELYON, 69626 Villeurbanne, France;

[4] Shanghai Key Laboratory of Atmospheric Particle Pollution and Prevention (LAP[3]), Department of Environmental Science & Engineering, Jiangwan Campus, Fudan University, Shanghai 200438, China

[5] Collaborative Innovation Center on Forecast and Evaluation of Meteorological Disasters (CIC-FEMD), NUIST Center on Atmospheric Environment, Nanjing University of Information Science and Technology, Nanjing 210044, China

Corresponding authors: Cheng Huang (huangc@saes.sh.cn)

ABSTRACT

18   Oxygenated organic molecules (OOMs) are dominated by the N-containing species in polluted urban

19   environment. As N-containing OOMs, especially those with more than one nitrogen atoms, prevailed in

20   the high m/z range (m/z > 350Th), unambiguous identification of N-containing OOMs is highly desirable

21   for understanding of their formation processes, precursors and influencing factors. To achieve this, we

22   applied an ultra-high-resolution chemical ionization-orbitrap (CI-Orbitrap) in a field campaign and found

23   that OOMs contain one (1N-OOMs), two (2N-OOMs) and three (3N-OOMs) nitrogen atoms respectively

24   comprised 50%, 26% and 4% of total OOMs. More interestingly, the fraction of 2N-OOMs increased with

25   the increase of carbon number (nC) and were dominated by the ones derived from aliphatic precursors

26   (2N-OOM$_{Ali}$, 64.2%), indicating the importance of multistep oxidation. Plausible precursors of 2N-OOMs

27   were aliphatics (2N-OOM$_{Ali}$, 64.2%), aromatics (2N-OOM$_{Aro}$, 16%), and monoterpenes (2N-OOM$_{MT}$,

28   15.4%). The absolute concentrations of 2N-OOMs were greatly affected by the pollution level for the most

29   cases. The 2N-OOM$_{Ali}$ was the most abundant 2N-OOMs and its fraction even increased in the polluted

30   day with enhanced proportion of the ones with nC>10. While 2N-OOM$_{Ali}$ and 2N-OOM$_{Aro}$ were

31   dominated by daytime photochemical production, nighttime NO$_3$-initiated oxidation played a comparable

32   role as the daytime photochemistry in the formation of 2N-OOM$_{MT}$. 2N-OOM$_{Aro}$ were of highest

33   oxygenation level, followed by 2N-OOM$_{MT}$ and 2N-OOM$_{Ali}$, which were affected by photochemistry and

34   NO$_x$ concentrations. These results highlight the significant formation of 2N-OOMs and the influencing

35   factors, on their formation in polluted urban environment, where various VOC precursors and atmospheric

36   oxidants present.

1. Introduction

Secondary organic aerosol (SOA) accounts for a significant fraction of particulate matters (Donahue et al., 2009; Ehn et al., 2014; Hallquist et al., 2009; Jimenez et al., 2009). Volatile organic compounds (VOCs) and their oxidation products, *i.e.*, OVOCs, are important precursors of SOA in the atmosphere (Atkinson and Arey, 2003; Bianchi et al., 2019; Ehn et al., 2014; Nie et al., 2022). The N-containing oxygenated organic molecules (OOMs) have been identified as the important products upon VOC oxidation. Especially at high NO_x levels, these products become more dominant while the others (*i.e.*, alcohols, hydroperoxides and RO_2 cross-reaction products) are likely suppressed (Bianchi et al., 2019; Zhao et al., 2018). The nitrogen atoms in OOM molecules are assumed to be mainly associated with nitrate group ($-ONO_2$) formed from bi-molecular reaction between RO_2 radical and NO. Field measurements also observed that up to 77 % of molecules in organic aerosol (OA) contain nitrate functional groups under different atmospheric conditions (Ditto et al., 2020; Kenagy et al., 2021; Kiendler-Scharr et al., 2016; Lee et al., 2016; Ng et al., 2017; Lin et al., 2021; Rollins et al., 2013; Xu et al., 2015; Ye et al., 2021; Yu et al., 2019).

The N-containing OOM molecules can be classified into 1N-OOMs, 2N-OOMs, and 3N-OOMs, according to the number of N atoms in the molecule. The chemical composition of N- containing OOMs is determined by their precursors, formation pathways and NO_x level in the atmosphere (Bianchi et al., 2019; Ehn et al., 2014; Nie et al., 2022; Pye et al., 2019; Riva, 2016; Yan et al., 2016). Recent observations in megacities of China indicated that 2N-OOMs accounted for significant fractions (about 30-33%) among total N-containing OOMs besides 1N-OOMs (66-70%) due to the high NO_x concentrations in polluted urban environment (Nie et al., 2022; Yan et al., 2021). Some laboratory studies also proposed that the potential formation pathways of 2N-OOMs, such as the multiple-step OH oxidation (Garmash et al., 2020) or the NO_3-initiated oxidation followed by NO termination (Kiendler-Scharr et al., 2016; Liebmann et al., 2019), suggesting the increased importance of multi-step bimolecular oxidation in the formation of 2N-OOMs. On the other hand, it was also found that the formation of 2N-OOMs showed the clear preference of specific precursors compared to 1N-OOMs, *i.e.*, significantly higher branch ratio of 2N-OOMs from

aliphatic hydrocarbons than those from aromatics (Nie et al., 2022), suggesting considerable difference from 1N-OOMs in terms of formation pathway. Determining the formation pathway of N-containing OOM molecules, especially those containing two to three nitrogen atoms, in real atmosphere, is challenging. Identification of their chemical compositions in molecular level is the key for advancing our understanding in the precursor, formation and sources of N-containing OOMs in polluted atmosphere, where thousands of oxidation products exist and evolve constantly.

Traditionally, a chemical ionization atmospheric pressure interface time-of-flight mass spectrometer (CI-APi-TOF) has been used to measure the gaseous OOMs (Berndt et al., 2016; Ehn et al., 2014; Jokinen et al., 2014; Rissanen et al., 2014). Using a CI-APi-TOF, increasing number of studies have been reporting the formation of OOMs through the oxidation of various VOC precursors in chamber or flow tube (Berndt et al., 2016, 2018; Ehn et al., 2014; Garmash et al., 2020; Jokinen et al., 2014, 2015; Rissanen et al., 2014; Wang et al., 2020; Zhao et al., 2018). While 2N-OOMs in real ambient almost exclusively located in high m/z (mass-to-charge) range (*i.e.*, 300 - 500 Th), a CI-APi-TOF with highest mass resolving power of 12,000 (m/Δm, in full width at half maximum) at m/z=200 Th and above, can hardly identify the molecular compositions of 2N-OOMs unambiguously. This is because low mass resolving power imposes significant uncertainties on separating overlapping peaks, which increases rapidly with increasing m/z and decreasing mass resolving power. Taken the integer m/z of 342 as an example, multiple peaks overlap at this nominal mass, *i.e.*, $C_7H_8O_{10}N_2(NO_3)^-$ (342.0057 Th), $C_8H_{12}O_9N_2(NO_3)^-$ (342.0421 Th), $C_9H_{16}O_8N_2(NO_3)^-$ (342.0785 Th), $C_{10}H_{20}O_7N_2(NO_3)^-$ (342.1149 Th). The adjacent peaks are of mass differences (Δm) of 0.0364 and a good peak separation of these peaks (4σ) requires mass resolving power of at least 16,000. Therefore, development and application of mass spectrometry techniques with extremely high performance in detection limit, time resolution, and mass resolving power, are highly desirable.

To achieve accurate identification of molecular formula from the extremely complex mass spectra, a CI (nitrate) inlet had also been coupled to an orbitrap mass spectrometer (CI-Orbitrap) to measure the OOMs in ultra-high mass resolving power (m/Δm> 100,000 at m/z=200-500 Th) (Riva et al., 2019a; Zhang et al., 2022). The ultra-high mass resolving power of CI-Orbitrap will undoubtedly provide

significant improvements in molecular identification, separation, and quantification. Herein, we applied a CI-Orbitrap in a field campaign for the measurements of OOMs, with a special focus on 2N-OOMs, in molecular level in urban Shanghai. The site represents a typical eastern Chinese megacity characterized by intense human activities, multiple anthropogenic emissions and high NO_x concentrations. Based on the measurement results as well as our current knowledge on N-containing OOM formation, we classify the observed 2N-OOMs into different precursor groups and explore the potential influencing factors on their formation. Furthermore, supported by positive matrix factorization (PMF), sources and gas-phase oxidation processes for 2N-OOM formation in urban Shanghai were identified.

2. Ambient measurement and methodology

2.1 Measurements

The field campaign was carried out from 31th October to 18th November, 2020 on the top-floor of an 8-story building in Shanghai Academy of Environmental Sciences (31°18' N, 121°43' E, Figure S1), which sits in a densely populated region surrounded by commercial properties and residential dwellings without significant industrial sources nearby. The site can represent a typical urban area of Shanghai affected by severe local emissions from vehicular traffic, commercial, and residential activities. Our campaign was carried out in autumn which represents a typical transition period from strong photochemistry in summer to intense regional transport in winter. At times, air masses transported from the neighboring provinces or even further from the northern China can also affect the air quality of the site.

The 2N-OOMs as well other OOMs molecules were measured in real time with a nitrate-Orbitrap. The operation of nitrate-Orbitrap has been detailed in previous studies as well as in one of our companion studies (Zhang et al., 2022), thus is only briefly described here. Ambient air was drawn into the ionization source through a 1m stainless-steel tube (3/4 inch). The reagent ion was produced by passing nitric acid in sheath flow (20L/min) into a PhotoIonizer (Model L9491, Hamamatsu, Japan) and was then introduced into a co-axial laminar flow reactor, in which the reagent ions interact with the air samples. The charged species were detected by an orbitrap mass analyzer with a mass resolving power of about 140,000. Mass-dependent transmission calibrations was also performed using a depletion method (Heinritzi et al., 2016).

Other ancillary measurements, including the PM$_{2.5}$ concentrations, trace gases (SO$_2$, O$_3$ and NO$_x$), volatile organic compounds, as well as meteorological parameters (wind direction and speed, solar radiation, etc.) were detailed in Supporting Information (SI-1). An overview of the measurement data, illustrating the air quality as well as the meteorological conditions during the campaign, is provided in SI-2 and Figure S2.

2.2 Data analysis of nitrate CI-Orbitrap

The raw mass spectra were first extracted by Orbitool (Cai et al., 2020) and the molecular information was then achieved by applying a homemade toolkit based on the MATLAB software. The toolkit drew on the idea from "tofTools" package which is used for analyzing the mass spectral data obtained from the TOF analyzer, such as nitrate CI-API-TOF (Junninen et al., 2010). The concentrations of the detected species are then determined as follows:

$$[X] = \frac{i[X^-]}{NO_3^- \cdot (HNO_3)_{0-2}} \cdot C \quad (1)$$

where $i[X^-]$ is the transmission-corrected signal intensity of ion X in unit of counts per second (cps), C represents the calibration factor. C is determined from the collision frequency of target species with the nitrate ions (cluster) during its residence in the charger, taking into account of the losses onto the walls of the reactor and the tube (Eq. 2):

$$C = C_{H2SO4} = \frac{1}{k_{ion} \times RT \times f_{inlet}} \quad (2)$$

where k_{ions} is the ion collision frequency in the range of $(1.7 - 2.3) \times 10^{-9}$ cm^3 s^{-1} (Ehn et al., 2014); RT is the residence time in the charger and f_{inlet} represents the fractions of target species that passed through the inlet.

Herein, we apply the C determined for sulfuric acid (H$_2$SO$_4$) of 3.4×10^9 molecules cm^{-3} ncps^{-1} to semi-quantify the concentrations of OOMs, which is widely used in previous studies (Ehn et al., 2014; Yan et al., 2021; Yao et al., 2018). Among the low volatility vapors, it had been demonstrated that nitrate ions exhibit highest charging efficiency toward H$_2$SO$_4$ (Ehn et al., 2014; Hyttinen et al., 2015, 2018; Riva et al., 2019b). The estimated concentrations of OOMs thus can be considered as the lower limits with an uncertainty of $\pm 50\%$ according to error propagation (Ehn et al., 2014). Positive matrix factorization (PMF) was also performed for the measured species using Source Finder (SoFi, v6.3) based on Igor and run by

141   the multilinear engine (ME-2) as detailed in SI-S3 and Figure S3-S6 (Canonaco et al., 2013).

3. Results and discussion

3.1 Chemical characteristic of OOMs

144   In total, we have identified 562 OOMs, which concentrated in the nC range of 5 to 10, taking up 84.6%

145   of total OOMs during the whole campaign (unless otherwise stated, all the reported values hereafter were

146   corresponding to the average of the whole campaign). Possible precursors of C_{5-10} OOMs include isoprene

147   (C_5), benzene/alkyl benzenes (C_{6-10}), aliphatic VOCs (C_{5-10}) and monoterpene (C_{10}) according to previous

148   studies (Bianchi et al., 2019; Nie et al., 2022). $C_{\leq 4}$ OOMs only took up a small fraction of 6.7% among

149   total OOMs and were likely a result of the decomposition from OOMs with large carbon numbers as

150   suggested by one of our companion studies (Zhang et al., 2022). The rest 8.7% were $C_{>10}$ OOMs which

151   accounted for a dominating fraction (70%, Figure S7) among the extremely low-volatility organic

152   compounds (ELVOC, $C^* < 3 \times 10^{-5}$ μg m^{-3}) based on a volatility parameterization proposed by Donahue

153   and co-workers (Donahue et al., 2011, 2012; Schervish and Donahue, 2020), and potentially poses larger

154   impacts on SOA formation owing to their lower volatility.

155   We further classified the detected OOMs into four groups based on the number of N atoms they

156   possessed, including non-nitrogen (0N-) OOMs, 1N-OOMs, 2N-OOMs, and 3N-OOMs. Their average

157   fractional contributions to total OOM concentrations as well as the carbon number (nC) distributions are

158   shown in Figure 1. We found 1N-OOMs dominated the total OOM concentration with an average fraction

159   of 50%, followed by 2N-OOMs (26%), demonstrating the dominance of N-containing OOMs among total

160   OOMs. The 3N-OOMs only took up a small fraction (4%) of total OOMs and the rest 20% was 0N-OOMs.

161   More interestingly, we found 1N-OOMs prevailed among the OOMs with nC $\leq$ 10, yet 2N-OOMs

162   dominated the $C_{>10}$ OOMs (41.8-84.2%), suggesting the increased importance of multi-step bimolecular

163   oxidation in the formation of 2N-OOMs with nC>10. We also note that the fraction of 2N-OOMs increased

164   stepwise with the increase of nC (Figure 1b) while 3N-OOMs don't exhibit a similar dependence. The

165   potential reason is that, with the increase of nC, on the one hand, more active sites are potentially provided

166   to promote the occurrence of multi-step oxidation, but on the other hand, the potential larger steric effect

can hinder multi-step oxidation. From our observation, these two factors lead an overall positive coupling for 2N-OOMs, but result in a non-monotonic trend for 3N-OOMs. Furthermore, these 2N-OOMs with nC>10 had an average molecular composition of $C_{12.5}H_{22.7}O_{2.1}(NO_3)_2$. Assuming the nitrogen atoms are only associated with nitrate group ($-ONO_2$), the mean double bond equivalent value (DBE) (Nie et al., 2022; Xu et al., 2021) was 1.15 on the carbon skeleton, suggesting its origination from aliphatic compounds, such as alkanes, alkenes, etc. (Gong et al., 2005; Mentel et al., 2015; Wang and Hildebrandt Ruiz, 2018).

We thus further classified the 2N-OOMs to their possible VOC precursors following a recently developed workflow proposed by Nie and co-workers, which is based on the up-to-date understanding of VOC oxidation and molecular characters (*i.e.,* number of different elements, DBE) as well as PMF results (Nie et al., 2022), *i.e.*, aromatics (2N-OOM$_{Aro}$), aliphatics (2N-OOM$_{Ali}$), and monoterpene (2N-OOM$_{MT}$). Note that we group isoprene 2N-OOMs (2N-OOM$_{Iso}$) into 2N-OOM$_{Ali}$ as well because of the low concentration of isoprene in cold season. As a result, the average fractions of 2N-OOM$_{Aro}$, 2N-OOM$_{Ali}$ and 2N-OOM$_{MT}$ among total 2N-OOMs were 16.0%, 64.2% and 15.3%, respectively (Figure 2), suggesting significant contribution of aliphatic compounds to 2N-OOMs formation. Taken together, the increased fraction of 2N-OOMs with the increase of nC and the dominant fraction of 2N-OOM$_{Ali}$ highlight the significant contribution of high-molecular-weight aliphatic precursors (*i.e.*, intermediate volatility or semi-volatile organic compounds, I/SVOCs) to high-molecular-weight 2N-OOM formation, which were potentially important SOA material. We thus focus our attention on the formation of 2N-OOMs in the following sections.

3.2 2N-OOM formation in PM episodes

To investigate the formation mechanisms and factors that may affect the 2N-OOM formation, one clean day (4th-5th November) and one polluted day (7th-8th November) based on the pollution levels, *i.e.*, PM$_{2.5}$ concentrations, were selected for further analysis. Since OOM formation is directly mediated by photochemistry or nighttime chemistry, the clean and polluted cases were thus split into one clean daytime case (CL$_{day}$), one clean nighttime case (CL$_{night}$), one polluted daytime case (PL$_{day}$) and one polluted

193 nighttime case (PL_{night}). Detailed information on durations, pollution levels, meteorological conditions

194 and 2N-OOM concentrations during these four cases were summarized in Table 1.

195   During the whole campaign, the concentrations of 2N-OOMs ranged from 1.1×10^6 to 42.0×10^6

196 molecule cm^{-3} as shown in Figure 2. We found the concentrations of 2N-OOMs in the polluted cases were

197 1.7-2.7 times higher than those in clean cases. Table 1 further indicates that the absolute abundances of

198 almost 2N-OOM classes were higher during the polluted cases as compared to clean case no matter in the

199 daytime or nighttime except for the daytime $2N\text{-}OOM_{Aro}$. Specifically, $2N\text{-}OOM_{Ali}$ occupied the largest

200 fractions, which were even higher in polluted cases (66-66%) than those in clean cases (56-61%, Figure

201 2). Especially for the $2N\text{-}OOM_{Ali}$ with nC>10, its concentration in polluted cases increased by a factor of

202 2.3-4.8 compared to the clean cases (Figure 3). From PMF analysis, we also identified a factor

203 characterized by a series of $2N\text{-}OOM_{Ali}$ (*i.e.*, $C_nH_{2n-2}O_8N_2$, n=5-11) as the fingerprint molecules (Table

204 S1). This factor tracks the $PM_{2.5}$ concentration well especially during PM episodes (Figure S8), likely due

205 to the availability of adequate aliphatic precursors during pollution episode. Furthermore, $2N\text{-}OOM_{Ali}$

206 with nC>10 presented both higher concentrations and fractions during daytime than nighttime cases

207 (Figure 3), suggesting that the photochemical formation of $2N\text{-}OOM_{Ali}$ prevailed compared to nighttime

208 formation. To compare CL_{night} and PL_{night}, it was also found that the pollution case would lead enhanced

209 importance of nighttime formation pathways of $2N\text{-}OOM_{Ali}$ with nC>10.

210   We note that the fraction of $2N\text{-}OOM_{Ali}$ increased during CL_{night} primarily due to the more evident

211 decrease of $2N\text{-}OOM_{Aro}$ (Table 1), whose formation is dominated by photochemistry. On the other hand,

212 the decrease of $2N\text{-}OOM_{Aro}$ concentrations at PL_{night} was not as obvious as those on CL_{night}. Due to the

213 significant increase of $2N\text{-}OOM_{Ali}$ concentration, the fraction of $2N\text{-}OOM_{Aro}$ decreased in pollution cases,

214 but their absolute concentrations only had few changes in the daytime. $2N\text{-}OOM_{MT}$ showed significant

215 higher concentrations but similar fractions in polluted cases. On the other hand, equivalent or even slightly

216 higher concentrations during nighttime than those in daytime suggest the comparable importance of

217 nighttime chemistry in $2N\text{-}OOM_{MT}$ formation in contrast to $2N\text{-}OOM_{Ali}$ and $2N\text{-}OOM_{Aro}$, which will be

218 discussed in later sections.

219   To summarize, the absolute concentrations of 2N-OOM were greatly affected by the pollution level

220   for the most cases. Both the concentrations and fractions of 2N-OOM$_{Ali}$ were significantly promoted by

221   pollution condition, whereas the 2N-OOM$_{Aro}$ were predominantly affected by photochemical production,

222   whose formation was less sensitive to pollution levels compared to 2N-OOM$_{Ali}$ in the daytime. In contrast,

223   the absolute concentrations of 2N-OOM$_{MT}$ were also significantly influenced by pollution levels but seem

224   not solely/almost depend on daytime/nighttime formation pathway. In addition, we note that both daytime

225   photochemistry and nighttime chemistry had profound effects on 2N-OOMs formation under different

226   pollution levels, presumably depending on availability of the precursors as well as the oxidants. We thus

227   focus our attention on the formation of 2N-OOMs during daytime versus nighttime in the following

228   sections.

229   **3.3 Daytime vs. nighttime formation of 2N-OOMs**

230   We thus investigate the effects of photochemistry and nighttime chemistry on the formation of

231   individual 2N-OOMs. While the former is dominated by OH radical oxidation, the latter involves NO$_3$

232   radical oxidation as well as reactions with ozone or other oxidants, *e.g.*, halogen. Herein, we use solar

233   radiation as a proxy of photochemical reactivity, and the concentrations of NO$_3$ radical were estimated

234   assuming that NO$_3$, NO$_2$ and N$_2$O$_5$ were under fast equilibration in troposphere (Brown and Stutz, 2012).

235   The correlation coefficients (Spearman type) between individual 2N-OOM molecules and solar radiation

236   ($R_{2N\text{-}OOMs\text{-}solar}$) or NO$_3$ radical ($R_{2N\text{-}OOMs\text{-}NO3}$) derived from different precursors during the whole campaign

237   were shown in Figure 4a. It should be noted that the concentrations of 2N-OOMs and NO$_3$ radicals were

238   scaled with the boundary layer height before calculating the correlation coefficients here and below for

239   correcting the effects of meteorological dilution.

240   Both 2N-OOM$_{Aro}$ and 2N-OOM$_{Ali}$ showed stronger correlations with solar radiation over NO$_3$

241   radicals, indicating their association with daytime photochemistry since benzene/alkyl benzenes and

242   aliphatic VOCs rapidly react with OH radicals compared to other oxidants, such as NO$_3$ radicals. This is

243   also supported by the observation that both 2N-OOM$_{Aro}$ and 2N-OOM$_{Ali}$ peaked during noontime (12:00-

244   14:00) as shown in Figure 4b. Similarly, the PMF analysis also distinguished two daytime factors. The

daytime factor-1 peaked at around 12:00-14:00 (Table S1) and highly correlated with solar radiation (R=0.57). The fingerprint-molecules of daytime factor-1 are $C_nH_{2n-4}O_{10}N_2$ (n=8-10) with average DBE values of 2 on the carbon skeleton, suggesting the dominance of 2N-OOMs likely formed from aromatic precursors. Since each step of OH oxidation of aromatics followed by RO_2+NO_x termination would increase the nH by one, this factor is likely dominated by 2N-OOMs formed from two steps of OH-initiated oxidation from alkylbenzenes given the carbon numbers ranged from 8 to 10.

The key fingerprint molecule of daytime factor-2 is $C_nH_{2n}O_8N_2$ (n=4-5) (accounting for 30.8% in the factor profile), followed by $C_nH_{2n-2}O_8N_2$ (n=5-6) (accounting for 9.7% in the factor profile), which is likely a result of the decomposition from 2N-OOM$_{Ali}$ with large carbon numbers, according to their DBE values of 0-1 on the carbon skeleton. This aliphatic factor presented even higher correlation with solar radiation (R=0.65), peaking at around 12:00-14:00. Strong daytime peaks together with the good correlations with irradiation suggest the dominance of photochemical oxidation in the formation of 2N-OOM$_{Ali}$. For 2N-OOM$_{Ali}$, although it showed strong daytime peak, weak nighttime peak was still observed. This indicates that although daytime formation of 2N-OOM$_{Ali}$ prevails, their nighttime formation still existed. For example, we have obtained a nighttime factor from PMF analysis (nighttime factor-2), whose fingerprint molecules are $C_5H_8O_9N_2$ and $C_nH_{2n}O_7N_2$ (n=5-8). $C_5H_8O_9N_2$ was likely originated from isoprene and $C_nH_{2n}O_7N_2$ were likely from anthropogenic aliphatic precursors.

Nighttime chemistry plays a more important role in the formation of 2N-OOM$_{MT}$. This is further supported by the slightly stronger correlation between 2N-OOM$_{MT}$ and NO_3 radicals than solar radiation. For some specific 2N-OOM$_{MT}$ species, the formation is likely a result of NO_3 radical initiated oxidation. As shown in Figure 5, we have identified a series of 2N-OOM$_{MT}$ molecules with molecular composition of $C_{10}H_{16}O_{7,9,11}N_2$, which showed strong positive correlations with NO_3 radical. The occurrence of propagation reaction from RO_2 to RO was critical to the formation of odd oxygen as proposed in previous chamber studies (Boyd et al., 2015; Claflin and Ziemann, 2018). Furthermore, under the nighttime conditions observed in urban Shanghai (Table 1), it is estimated that monoterpenes primarily react with NO_3, and the fate of nighttime RO_2s is dominated by NO, which is clear different from rural

271   environment where NO levels likely drop to near zero after sunset (Romer et al., 2016) and RO_2s are likely

272   terminated by NO_3-RO_2 cross-reactions (Bates et al., 2022). Therefore, formation of $C_{10}H_{16}O_{7,9,11}N_2$ likely

273   started with the reaction of monoterpene with NO_3 radicals forming a NO_3-$C_{10}H_{16}$ alkyl radical, followed

274   by the formation of organic peroxy radical (RO_2) upon addition of O_2. The RO_2 is then converted to an

275   alkoxy radical (RO) upon reaction with NO. The autoxidation process would then start and stepwise

276   introduce O_2 into the molecule, forming a series of more oxygenated RO_2 radicals, *i.e.*, NO_3-

277    $C_{10}H_{16}(O)(OO)_n$. The NO termination reaction of these RO_2 radicals would finally result in ONs with

278   chemical composition of NO_3-$C_{10}H_{16}(O)(OO)_nO(NO)O$ (n=0, 1, 2).

279   On the other hand, the reaction rate between monoterpenes (i.e., alpha-pinene, beta-pinene and

280   limonene) and NO_3 are about 60,000-140,000 times faster than that between monoterpenes and O_3 at 293K

281   (MCMv3.1), but the averaged nighttime concentrations of O_3 (22.8 ppb) was only about 18,000 times

282   higher than that of NO_3 (1.3 ppt). Therefore, NO_3-initiated oxidation process posed significant impacts on

283   2N-OOM$_{MT}$ formation during nighttime. The 2N-OOM$_{MT}$ resulted from NO_3 oxidation is also resolved as

284   a nighttime factor (nighttime factor-1) from PMF analysis, which tracked the NO_3 concentrations well

285   (Figure S9, *R*=0.46) and peaked at around 19:00-23:00. Fingerprint molecule of nighttime factor-1 was

286   mainly including $C_{10}H_{16}O_9N_2$ and $C_{10}H_{16}O_8N_2$, which is generated from NO_3-initiated oxidation followed

287   by NO termination and this process will not change the nH of the parent monoterpene molecule.

288   **3.4 Oxygenation level of 2N-OOMs**

289   We then calculated the average effective oxygen number (nO_{eff}= nO - 2nN) of 2N-OOMs, which is

290   used to indicate the oxidation state of carbon by excluding the oxygen atoms bonded with nitrogen atoms.

291   Note that calculation of nO_{eff} assumes that the nitrogen atoms are only associated with nitrate group (-

292   ONO_2), which is reasonable after excluding nitrophenol peaks. The average nO_{eff} of 2N-OOMs from

293   different precursors in CL_{day}, CL_{night}, PL_{day} and PL_{night} were shown in Figure 6 and summarized in Table

294   S2. 2N-OOM$_{Aro}$ had the highest nO_{eff} (4.8-5.6), followed by 2N-OOM$_{MT}$ (4.5-4.9) and 2N-OOM$_{Ali}$ were

295   of lowest nO_{eff} (3.9-4.0). Difference in the oxygenation level of different types of OOMs can be attributed

296   to the difference in oxidation mechanisms of the initiation reactions. For example, the OH-initiated

297 oxidation of alkanes, aromatics and monoterpene/alkenes would form a $C_xH_yO_2$ radical, $C_xH_yO_5$ radical

298 and $C_xH_yO_3$ radical, respectively, incorporating different number of oxygen atoms into the original

299 precursor molecules at the first step of oxidation (MCMv3.1). On the other hand, during the multiple-step

300 oxidation in daytime, aromatics could still provide more C=C bonds than other precursors after the initial

301 step which is plausibly capable to further react with OH, O_3 and others oxidants.

302   Furthermore, we also found that regardless of the pollution level, the nO_{eff} was considerably higher

303 in daytime cases than that in nighttime cases particularly for 2N-OOM$_{Aro}$ and 2N-OOM$_{MT}$, suggesting a

304 profound effects of photochemistry on the formation of highly oxygenated 2N-OOMs. This is likely

305 because of the high NO_x concentrations during the nighttime (Table 1), which could efficiently suppress

306 the RO_2 radicals from autoxidation reactions forming overall less oxygenated OOM molecules. The effect

307 of NO_x on oxygenation levels would be discussed in a subsequent paragraph. The average nO_{eff} of 2N-

308 OOM$_{Ali}$ in four sub-periods were similar without significant daytime and nighttime difference, ranging

309 from 3.9-4.0. This could be partly explained by the fact that reactions with oxidants such as OH and

310 halogen radicals will similarly result in the addition of oxygen atoms by two for alkanes during the first

311 step of oxidation. Thus, the oxygenation levels of 2N-OOM$_{Ali}$ were supposed to be insensitive to the

312 oxidants in daytime or nighttime.

313   It is known that NO is also critical in determining the fate of RO_2 radical during the oxidation,

314 forming RO radicals or organonitrates. Formation of RO radicals and organonitrates will have opposite

315 effects on the oxidation state of the termination products since the former will significantly increase the

316 oxygenation state of carbon through initiating propagation reactions before termination. We thus explore

317 the effects of NO as well as the total NO_x concentrations on the average oxygenation levels of 2N-OOMs

318 from different precursors during the whole campaign (Figure 7). Consistent with previous studies in

319 polluted urban environment (Qiao et al., 2021; Yan et al., 2021), the detected 2N-OOMs were also of low

320 oxygenation with nO_{eff} of 3.9-5.4 (25-75% percentile) compared to those measured in forest or in

321 laboratory studies (Berndt et al., 2016; Ehn et al., 2014; Jokinen et al., 2014; Rissanen et al., 2014; Yan et

322 al., 2016). nO_{eff} of 2N-OOM$_{Aro}$ and 2N-OOM$_{MT}$ increased with the decrease of NO/NO_x concentrations.

323 This is likely due to the prevailing of NO termination reactions because the maximum autoxidation rate

324 constant of alkylbenzenes with long-chain substituents (e.g., isopropyl-benzene, ethyl-benzene) and

325 monoterpene are comparable to the bimolecular reaction rate between RO_2 and NO (Bianchi et al., 2019).

326 The oxygenation levels of 2N-OOM$_{Ali}$ appears to be insensitive to the pollution levels and NO/NO$_x$

327 concentrations, which should be further investigated in future studies.

4 Conclusion

329 We report the unambiguous identification of 2N-OOMs as well as other OOMs using an ultra-high-

330 resolution orbitrap coupled with a nitrate inlet. We found that OOMs distributed in a wide range of carbon

331 numbers (nC = 4 - 16), among which the 2N-OOMs occupied a considerable fraction (26%) of the total

332 observed OOMs. During the whole campaign, the 2N-OOM concentrations ranged from 1.1×10^6 to

333 42.0×10^6 molecule cm^{-3} and concentrated in the nC range of 5 to 10 with high molecular weight (m/z >

334 350 Th), suggesting their low volatilities and thus potentially high contribution to local SOA formation.

335 Aliphatic, aromatics, and monoterpenes were plausible precursors of 2N-OOMs with a fraction of

336 64.2%, 16% and 15.4%, respectively. The absolute concentrations of 2N-OOMs were greatly affected by

337 the pollution level for the most cases. The 2N-OOM$_{Ali}$ was found to be the most abundant 2N-OOMs and

338 its fraction even increased in the polluted day with enhanced proportion of ones with nC>10, probably

339 due to the high concentrations of aliphatic precursors accompanied with PM episodes. Significant

340 contribution of long-chain aliphatic compounds (nC > 10) to 2N-OOM formation is also supported by the

341 observation that 2N-OOM fraction increased with the increase of nC and they are of low DBE values,

342 likely through multistep bimolecular oxidation. 2N-OOM$_{Ali}$ and 2N-OOM$_{Aro}$ mainly peaked in daytime

343 and showed stronger correlations with solar radiation over NO$_3$ radicals, indicating their association with

344 daytime photochemistry since benzene/alkyl benzenes and aliphatic hydrocarbons rapidly react with OH

345 radicals compared with other oxidants, such as NO$_3$ radicals. In contrast, 2N-OOM$_{MT}$ prevailed both in

346 daytime and nighttime, some specific 2N-OOM$_{MT}$ species showed strong positive correlations with NO$_3$

347 radical and were likely a result of NO$_3$ radical initiated oxidation, suggesting the comparable importance

348 of nighttime NO$_3$ chemistry in 2N-OOM$_{MT}$ formation. In terms of oxygenation levels, we found that 2N-

349   OOM_{Aro} had highest averaged nO_{eff} followed by $2N\text{-}OOM_{MT}$. Daytime photochemistry and low NO_x

350   concentrations had profound effects on the formation of more oxygenated 2N-OOMs. $2N\text{-}OOM_{Ali}$ had the

351   lowest nO_{eff} and had negligible changes under different pollution levels. These results demonstrate the

352   preference of 2N-OOM formation and the influencing factors in a Chinese megacity involving various

353   VOC precursors (biogenic VOCs such as monoterpene and anthropogenic VOCs such as aromatics,

354   aliphatic hydrocarbons) and various atmospheric oxidants (such as OH radical and NO_3 radicals), and

355   highlight the influence of PM episode.

356 **Code/Data availability**

357   Data presented in this paper are available upon request to the corresponding author.

358 **Author contributions**

359   CH designed this study. YL, YM, DDH, SL, SJ, and YG conducted the field campaign. YL analyzed

360 data with contributions from CH and all the other co-authors. YL wrote the manuscript with contributions

361 from all the other co-authors.

362 **Competing interests**

363   The authors declare that they have no conflict of interest.

364 **Acknowledgement**

365   This study was financially supported by the National Key R&D Program of China

366 (2022YFC3700205), and China Postdoctoral Science Foundation (2022T150427, 2022M712146).

367 # Reference

368 Atkinson, R. and Arey, J.: Atmospheric Degradation of Volatile Organic Compounds, Chem. Rev., 103(3),

369   4605–4638, doi:10.1021/cr0206420, 2003.

370 Bates, K. H., Burke, G. J. P., Cope, J. D. and Nguyen, T. B.: Secondary organic aerosol and organic

371   nitrogen yields from the nitrate radical (NO3) oxidation of alpha-pinene from various RO2 fates,

372   Atmos. Chem. Phys., 22(2), 1467–1482, doi:10.5194/acp-22-1467-2022, 2022.

373 Berndt, T., Richters, S., Jokinen, T., Hyttinen, N., Kurtén, T., Otkjær, R. V., Kjaergaard, H. G., Stratmann,

374   F., Herrmann, H., Sipilä, M., Kulmala, M. and Ehn, M.: Hydroxyl radical-induced formation of

375   highly oxidized organic compounds, Nat. Commun., 7(13677), doi:10.1038/ncomms13677, 2016.

376 Berndt, T., Scholz, W., Mentler, B., Fischer, L., Herrmann, H., Kulmala, M. and Hansel, A.: Accretion

377   Product Formation from Self- and Cross-Reactions of RO2 Radicals in the Atmosphere, Angew.

378   Chemie - Int. Ed., 57(14), 3820–3824, doi:10.1002/anie.201710989, 2018.

379 Bianchi, F., Kurtén, T., Riva, M., Mohr, C., Rissanen, M. P., Roldin, P., Berndt, T., Crounse, J. D.,

380   Wennberg, P. O., Mentel, T. F., Wildt, J., Junninen, H., Jokinen, T., Kulmala, M., Worsnop, D. R.,

381   Thornton, J. A., Donahue, N., Kjaergaard, H. G. and Ehn, M.: Highly Oxygenated Molecules (HOM)

382   from Gas-Phase Autoxidation Involving Organic Peroxy Radicals: A Key Contributor to

383   Atmospheric Aerosol, Chem. Rev., 119, 3472–3509, doi:10.1021/acs.chemrev.8b00395, 2019.

384 Boyd, C. M., Sanchez, J., Xu, L., Eugene, A. J., Nah, T., Tuet, W. Y., Guzman, M. I. and Ng, N. L.:

385   Secondary organic aerosol formation from the β-pinene+NO3 system: Effect of humidity and peroxy

386   radical fate, Atmos. Chem. Phys., 15(13), 7497–7522, doi:10.5194/acp-15-7497-2015, 2015.

387 Brown, S. S. and Stutz, J.: Nighttime radical observations and chemistry, Chem. Soc. Rev., 41, 6405–

388   6447, doi:10.1039/c2cs35181a, 2012.

389 Cai, R., Li, Y., Clément, Y., Li, D., Dubois, C., Fabre, M., Besson, L., Perrier, S., George, C., Ehn, M.,

390   Huang, C., Yi, P., Ma, Y. and Riva, M.: Orbitool: A software tool for analyzing online Orbitrap mass

391   spectrometry data, Atmos. Meas. Tech., 14, 2377–2387, doi:10.5194/amt-2020-267, 2020.

392 Canonaco, F., Crippa, M., Slowik, J. G., Baltensperger, U. and Prévôt, A. S. H. H.: SoFi, an IGOR-based

393   interface for the efficient use of the generalized multilinear engine (ME-2) for the source

394   apportionment: ME-2 application to aerosol mass spectrometer data, Atmos. Meas. Tech., 6(12),

395   3649–3661, doi:10.5194/amt-6-3649-2013, 2013.

396 Claflin, M. S. and Ziemann, P. J.: Identification and Quantitation of Aerosol Products of the Reaction of

397   β-Pinene with NO3 Radicals and Implications for Gas- and Particle-Phase Reaction Mechanisms, J.

398   Phys. Chem. A, 122(14), 3640–3652, doi:10.1021/acs.jpca.8b00692, 2018.

399 Ditto, J. C., Joo, T., Slade, J. H., Shepson, P. B., Ng, N. L. and Gentner, D. R.: Nontargeted Tandem Mass

400   Spectrometry Analysis Reveals Diversity and Variability in Aerosol Functional Groups across

Multiple Sites, Seasons, and Times of Day, Environ. Sci. Technol. Lett., 7(2), 60–69, doi:10.1021/acs.estlett.9b00702, 2020.

Donahue, N. M., Robinson, A. L. and Pandis, S. N.: Atmospheric organic particulate matter: From smoke to secondary organic aerosol, Atmos. Environ., 43(1), 94–106, doi:10.1016/j.atmosenv.2008.09.055, 2009.

Donahue, N. M., Epstein, S. A., Pandis, S. N. and Robinson, A. L.: A two-dimensional volatility basis set: 1. organic-aerosol mixing thermodynamics, Atmos. Chem. Phys., 11(7), 3303–3318, doi:10.5194/acp-11-3303-2011, 2011.

Donahue, N. M., Kroll, J. H., Pandis, S. N. and Robinson, A. L.: A two-dimensional volatility basis set-Part 2: Diagnostics of organic-aerosol evolution, Atmos. Chem. Phys., 12(2), 615–634, doi:10.5194/acp-12-615-2012, 2012.

Ehn, M., Thornton, J. A., Kleist, E., Sipilä, M., Junninen, H., Pullinen, I., Springer, M., Rubach, F., Tillmann, R., Lee, B., Lopez-Hilfiker, F., Andres, S., Acir, I.-H. H., Rissanen, M., Jokinen, T., Schobesberger, S., Kangasluoma, J., Kontkanen, J., Nieminen, T., Kurtén, T., Nielsen, L. B., Jørgensen, S., Kjaergaard, H. G., Canagaratna, M., Maso, M. D., Berndt, T., Petäjä, T., Wahner, A., Kerminen, V.-M. M., Kulmala, M., Worsnop, D. R., Wildt, J. and Mentel, T. F.: A large source of low-volatility secondary organic aerosol, Nature, 506(7489), 476–479, doi:10.1038/nature13032, 2014.

Garmash, O., Rissanen, M. P., Pullinen, I., Schmitt, S., Kausiala, O., Tillmann, R., Zhao, D., Percival, C., Bannan, T. J., Priestley, M., Hallquist, A. M., Kleist, E., Kiendler-Scharr, A., Hallquist, M., Berndt, T., McFiggans, G., Wildt, J., Mentel, T. F. and Ehn, M.: Multi-generation OH oxidation as a source for highly oxygenated organic molecules from aromatics, Atmos. Chem. Phys., 20(1), 515–537, doi:10.5194/acp-20-515-2020, 2020.

Gong, H., Matsunaga, A. and Ziemann, P. J.: Products and mechanism of secondary organic aerosol formation from reactions of linear alkenes with NO3 Radicals, J. Phys. Chem. A, 109(19), 4312–4324, doi:10.1021/jp058024l, 2005.

Hallquist, M., Wenger, J. C., Baltensperger, U., Rudich, Y., Simpson, D., Claeys, M., Dommen, J., Donahue, N. M., George, C., Goldstein, A. H., Hamilton, J. F., Herrmann, H., Hoffmann, T., Iinuma, Y., Jang, M., Jenkin, M. E., Jimenez, J. L., Kiendler-Scharr, A., Maenhaut, W., McFiggans, G., Mentel, T. F., Monod, A., Prévôt, A. S. H., Seinfeld, J. H., Surratt, J. D., Szmigielski, R. and Wildt, J.: The formation, properties and impact of secondary organic aerosol: Current and emerging issues, Atmos. Chem. Phys., 9(14), 5155–5236, doi:10.5194/acp-9-5155-2009, 2009.

Heinritzi, M., Simon, M., Steiner, G., Wagner, A. C., K??rten, A., Hansel, A. and Curtius, J.: Characterization of the mass-dependent transmission efficiency of a CIMS, Atmos. Meas. Tech., 9(4), 1449–1460, doi:10.5194/amt-9-1449-2016, 2016.

Hyttinen, N., Kupiainen-Määtta, O., Rissanen, M. P., Muuronen, M., Ehn, M. and Kurtén, T.: Modeling the Charging of Highly Oxidized Cyclohexene Ozonolysis Products Using Nitrate-Based Chemical Ionization, J. Phys. Chem. A, 119(24), 6339–6345, doi:10.1021/acs.jpca.5b01818, 2015.

Hyttinen, N., Otkjær, R. V., Iyer, S., Kjaergaard, H. G., Rissanen, M. P., Wennberg, P. O. and Kurtén, T.: Computational Comparison of Different Reagent Ions in the Chemical Ionization of Oxidized Multifunctional Compounds, J. Phys. Chem. A, 122(1), 269–279, doi:10.1021/acs.jpca.7b10015, 2018.

Jimenez, J. L., Canagaratna, M. R., Donahue, N. M., Prevot, A. S. H. H., Zhang, Q., Kroll, J. H., DeCarlo, P. F., Allan, J. D., Coe, H., Ng, N. L., Aiken, A. C., Docherty, K. S., Ulbrich, I. M., Grieshop, A. P., Robinson, A. L., Duplissy, J., Smith, J. D., Wilson, K. R., Lanz, V. A., Hueglin, C., Sun, Y. L., Tian, J., Laaksonen, A., Raatikainen, T., Rautiainen, J., Vaattovaara, P., Ehn, M., Kulmala, M., Tomlinson, J. M., Collins, D. R., Cubison, M. J., Dunlea, J., Huffman, J. A., Onasch, T. B., Alfarra, M. R., Williams, P. I., Bower, K., Kondo, Y., Schneider, J., Drewnick, F., Borrmann, S., Weimer, S., Demerjian, K., Salcedo, D., Cottrell, L., Griffin, R., Takami, A., Miyoshi, T., Hatakeyama, S., Shimono, A., Sun, J. Y., Zhang, Y. M., Dzepina, K., Kimmel, J. R., Sueper, D., Jayne, J. T., Herndon, S. C., Trimborn, A. M., Williams, L. R., Wood, E. C., Middlebrook, A. M., Kolb, C. E., Baltensperger, U., Worsnop, D. R., Dunlea, E. J., Huffman, J. A., Onasch, T. B., Alfarra, M. R., Williams, P. I.,

453   Bower, K., Kondo, Y., Schneider, J., Drewnick, F., Borrmann, S., Weimer, S., Demerjian, K.,

454   Salcedo, D., Cottrell, L., Griffin, R., Takami, A., Miyoshi, T., Hatakeyama, S., Shimono, A., Sun, J.

455   Y., Zhang, Y. M., Dzepina, K., Kimmel, J. R., Sueper, D., Jayne, J. T., Herndon, S. C., Trimborn, A.

456   M., Williams, L. R., Wood, E. C., Middlebrook, A. M., Kolb, C. E., Baltensperger, U. and Worsnop,

457   D. R.: Evolution of Organic Aerosols in the Atmosphere, Science (80-.)., 326(5959), 1525–1529,

458   doi:10.1126/science.1180353, 2009.

459 Jokinen, T., Sipilä, M., Richters, S., Kerminen, V. M., Paasonen, P., Stratmann, F., Worsnop, D., Kulmala,

460   M., Ehn, M., Herrmann, H. and Berndt, T.: Rapid autoxidation forms highly oxidized RO2 radicals

461   in the atmosphere, Angew. Chemie Int. Ed., 53, 14596–14600, doi:10.1002/anie.201408566, 2014.

462 Jokinen, T., Berndt, T., Makkonen, R., Kerminen, V.-M., Junninen, H., Paasonen, P., Stratmann, F.,

463   Herrmann, H., Guenther, A. B., Worsnop, D. R., Kulmala, M., Ehn, M. and Sipilä, M.: Production

464   of extremely low volatile organic compounds from biogenic emissions: Measured yields and

465   atmospheric implications, Proc. Natl. Acad. Sci., 112(23), 7123–7128,

466   doi:10.1073/pnas.1423977112, 2015.

467 Junninen, H., Ehn, M., Petäjä, Luosujärvi, L., Kotiaho, T., Kostiainen, R., Rohner, U., Gonin, M., Fuhrer,

468   K., Kulmala, M. and Worsnop, D. R.: A high-resolution mass spectrometer to measure atmospheric

469   ion composition, Atmos. Meas. Tech., 3(4), 1039–1053, doi:10.5194/amt-3-1039-2010, 2010.

470 Kenagy, H. S., Present, P. S. R., Wooldridge, P. J., Nault, B. A., Campuzano-jost, P., Day, D. A., Jimenez,

471   J. L., Zare, A., Pye, H. O. T., Yu, J., Song, C. H., Blake, D. R., Woo, J., Kim, Y. and Cohen, R. C.:

472   Contribution of Organic Nitrates to Organic Aerosol over South Korea during KORUS-AQ, Environ.

473   Sci. Technol., 55, 16326−16338, doi:10.1021/acs.est.1c05521, 2021.

474 Kiendler-Scharr, A., Mensah, A. A., Friese, E., Topping, D., Nemitz, E., Prevot, A. S. H., Äijälä, M.,

475   Allan, J., Canonaco, F., Canagaratna, M., Carbone, S., Crippa, M., Dall Osto, M., Day, D. A., De

476   Carlo, P., Di Marco, C. F., Elbern, H., Eriksson, A., Freney, E., Hao, L., Herrmann, H., Hildebrandt,

477   L., Hillamo, R., Jimenez, J. L., Laaksonen, A., McFiggans, G., Mohr, C., O'Dowd, C., Otjes, R.,

478   Ovadnevaite, J., Pandis, S. N., Poulain, L., Schlag, P., Sellegri, K., Swietlicki, E., Tiitta, P.,

479   Vermeulen, A., Wahner, A., Worsnop, D. and Wu, H. C.: Ubiquity of organic nitrates from nighttime

480   chemistry in the European submicron aerosol, Geophys. Res. Lett., 43(14), 7735–7744,

481   doi:10.1002/2016GL069239, 2016.

482 Lee, B. H., Mohr, C., Lopez-Hilfiker, F. D., Lutz, A., Hallquist, M., Lee, L., Romer, P., Cohen, R. C.,

483   Iyer, S., Kurtén, T., Hu, W., Day, D. A., Campuzano-Jost, P., Jimenez, J. L., Xu, L., Ng, N. L., Guo,

484   H., Weber, R. J., Wild, R. J., Brown, S. S., Koss, A., De Gouw, J., Olson, K., Goldstein, A. H., Seco,

485   R., Kim, S., McAvey, K., Shepson, P. B., Starn, T., Baumann, K., Edgerton, E. S., Liu, J., Shilling,

486   J. E., Miller, D. O., Brune, W., Schobesberger, S., D'Ambro, E. L. and Thornton, J. A.: Highly

487   functionalized organic nitrates in the southeast United States: Contribution to secondary organic

488   aerosol and reactive nitrogen budgets, Proc. Natl. Acad. Sci. U. S. A., 113(6), 1516–1521,

489   doi:10.1073/pnas.1508108113, 2016.

490 Ng, N., Brown, S. S., Archibald, A. T., Atlas, E., Cohen, R. C., Crowley, J. N., Day, D. A., Donahue, N.

491   M., Fry, J. L., Fuchs, H., Griffin, R. J., Guzman, M. I., Herrmann, H., Hodzic, A., Iinuma, Y.,

492   Kiendler-Scharr, A., Lee, B. H., Luecken, D. J., Mao, J., McLaren, R., Mutzel, A., Osthoff, H. D.,

493   Ouyang, B., Picquet-Varrault, B., Platt, U., Pye, H. O. T., Rudich, Y., Schwantes, R. H., Shiraiwa,

494   M., Stutz, J., Thornton, J. A., Tilgner, A., Williams, B. J. and Zaveri, R. A.: Nitrate radicals and

495   biogenic volatile organic compounds: Oxidation, mechanisms, and organic aerosol, Atmos. Chem.

496   Phys., 17(3), 2103–2162, doi:10.5194/acp-17-2103-2017, 2017.

497 Liebmann, J., Sobanski, N., Schuladen, J., Karu, E., Hellén, H., Hakola, H., Zha, Q., Ehn, M., Riva, M.,

498   Williams, J., Fischer, H., Lelieveld, J. and Crowley, J. N.: Alkyl nitrates in the boreal forest:

499   Formation via the NO3, OH and O3 induced oxidation of BVOCs and ambient lifetimes, Atmos.

500   Chem. Phys. Discuss., (3), 1–23, doi:10.5194/acp-2019-463, 2019.

501 Lin, C., Huang, R. J., Duan, J., Zhong, H. and Xu, W.: Primary and Secondary Organic Nitrate in

502   Northwest China: A Case Study, Environ. Sci. Technol. Lett., 8(11), 947–953,

503   doi:10.1021/acs.estlett.1c00692, 2021.

504 Mentel, T. F., Springer, M., Ehn, M., Kleist, E., Pullinen, I., Kurtén, T., Rissanen, M., Wahner, A. and

Wildt, J.: Formation of highly oxidized multifunctional compounds: autoxidation of peroxy radicals formed in the ozonolysis of alkenes-deduced from structure–product relationships, Atmos. Chem. Phys. Discuss., 15(2), 2791–2851, doi:10.5194/acpd-15-2791-2015, 2015.

Nie, W., Yan, C., Huang, D. D., Wang, Z., Liu, Y., Qiao, X., Guo, Y., Tian, L., Zheng, P., Xu, Z., Li, Y., Xu, Z., Qi, X., Sun, P., Wang, J., Zheng, F., Li, X., Yin, R., Dallenbach, K. R., Bianchi, F., Petäjä, T., Zhang, Y., Wang, M., Schervish, M., Wang, S., Qiao, L., Wang, Q., Zhou, M., Wang, H., Yu, C., Yao, D., Guo, H., Ye, P., Lee, S., Li, Y. J., Liu, Y., Chi, X., Kerminen, V.-M., Ehn, M., Donahue, N. M., Wang, T., Huang, C., Kulmala, M., Worsnop, D., Jiang, J. and Ding, A.: Secondary organic aerosol formed by condensing anthropogenic vapours over China's megacities, Nat. Geosci., 15, 255–261, doi:10.1038/s41561-022-00922-5, 2022.

Pye, H. O. T., D'Ambro, E. L., Lee, B. H., Schobesberger, S., Takeuchi, M., Zhao, Y., Lopez-Hilfiker, F., Liu, J., Shilling, J. E., Xing, J., Mathur, R., Middlebrook, A. M., Liao, J., Welti, A., Graus, M., Warneke, C., de Gouw, J. A., Holloway, J. S., Ryerson, T. B., Pollack, I. B. and Thornton, J. A.: Anthropogenic enhancements to production of highly oxygenated molecules from autoxidation, Proc. Natl. Acad. Sci. U. S. A., 116(14), 6641–6646, doi:10.1073/pnas.1810774116, 2019.

Qiao, X., Yan, C., Li, X., Guo, Y., Yin, R., Deng, C., Li, C., Nie, W., Wang, M., Cai, R., Huang, D., Wang, Z., Yao, L., Worsnop, D. R., Bianchi, F., Liu, Y., Donahue, N. M., Kulmala, M. and Jiang, J.: Contribution of Atmospheric Oxygenated Organic Compounds to Particle Growth in an Urban Environment, Environ. Sci. Technol., doi:10.1021/acs.est.1c02095, 2021.

Rissanen, M. P., Kurtén, T., Sipilä, M., Thornton, J. A., Kangasluoma, J., Sarnela, N., Junninen, H., Jørgensen, S., Schallhart, S., Kajos, M. K., Taipale, R., Springer, M., Mentel, T. F., Ruuskanen, T., Petäjä, T., Worsnop, D. R., Kjaergaard, H. G. and Ehn, M.: The formation of highly oxidized multifunctional products in the ozonolysis of cyclohexene, J. Am. Chem. Soc., 136(44), 15596–15606, doi:10.1021/ja507146s, 2014.

Riva, M.: Multiphase Chemistry of Highly Oxidized Molecules: The Case of Organic Hydroperoxides, Chem, 1(4), 526–528, doi:10.1016/j.chempr.2016.09.015, 2016.

531   Riva, M., Ehn, M., Li, D., Tomaz, S., Bourgain, F., Perrier, S. and George, C.: CI-Orbitrap: An Analytical

532   Instrument to Study Atmospheric Reactive Organic Species, Anal. Chem., 91, 9419–9423,

533   doi:10.1021/acs.analchem.9b02093, 2019a.

534   Riva, M., Rantala, P., Krechmer, J. E., Peräkylä, O., Zhang, Y., Heikkinen, L., Garmash, O., Yan, C.,

535   Kulmala, M., Worsnop, D. and Ehn, M.: Evaluating the performance of five different chemical

536   ionization techniques for detecting gaseous oxygenated organic species, Atmos. Meas. Tech., 12,

537   2403–2421, doi:10.5194/amt-2018-407, 2019b.

538   Rollins, A. W., Pusede, S., Wooldridge, P., Min, K. E., Gentner, D. R., Goldstein, A. H., Liu, S., Day, D.

539   A., Russell, L. M., Rubitschun, C. L., Surratt, J. D. and Cohen, R. C.: Gas/particle partitioning of

540   total alkyl nitrates observed with TD-LIF in Bakersfield, J. Geophys. Res. Atmos., 118(12), 6651–

541   6662, doi:10.1002/jgrd.50522, 2013.

542   Romer, P. S., Duffey, K. C., Wooldridge, P. J., Allen, H. M., Ayres, B. R., Brown, S. S., Brune, W. H.,

543   Crounse, J. D., De Gouw, J., Draper, D. C., Feiner, P. A., Fry, J. L., Goldstein, A. H., Koss, A.,

544   Misztal, P. K., Nguyen, T. B., Olson, K., Teng, A. P., Wennberg, P. O., Wild, R. J., Zhang, L. and

545   Cohen, R. C.: The lifetime of nitrogen oxides in an isoprene-dominated forest, Atmos. Chem. Phys.,

546   16(12), 7623–7637, doi:10.5194/acp-16-7623-2016, 2016.

547   Schervish, M. and Donahue, N. M.: Peroxy radical chemistry and the volatility basis set, Atmos. Chem.

548   Phys., 20(2), 1183–1199, doi:10.5194/acp-20-1183-2020, 2020.

549   Wang, D. S. and Hildebrandt Ruiz, L.: Chlorine-initiated oxidation of n-alkanes under high NOx

550   conditions: Insights into secondary organic aerosol composition and volatility using a FIGAERO-

551   CIMS, Atmos. Chem. Phys. Discuss., (x), 1–26, doi:10.5194/acp-2018-443, 2018.

552   Wang, Y., Mehra, A., Krechmer, J., Yang, G., Hu, X., Lu, Y., Lambe, A., Canagaratna, M., Chen, J.,

553   Worsnop, D., Coe, H. and Wang, L.: Oxygenated products formed from OH-initiated reactions of

554   trimethylbenzene: Autoxidation and accretion, Atmos. Chem. Phys., 20, 9563–9579,

555   doi:10.5194/acp-2020-165, 2020.

556   Xu, L., Suresh, S., Guo, H., Weber, R. J. and Ng, N. L.: Aerosol characterization over the southeastern

557   United States using high-resolution aerosol mass spectrometry: Spatial and seasonal variation of

558   aerosol composition and sources with a focus on organic nitrates, Atmos. Chem. Phys., 15(13), 7307–

559   7336, doi:10.5194/acp-15-7307-2015, 2015.

560 Xu, Z. N., Nie, W., Liu, Y. L., Sun, P., Huang, D. D., Yan, C., Krechmer, J., Ye, P. L., Xu, Z., Qi, X. M.,

561   Zhu, C. J., Li, Y. Y., Wang, T. Y., Wang, L., Huang, X., Tang, R. Z., Guo, S., Xiu, G. L., Fu, Q. Y.,

562   Worsnop, D., Chi, X. G. and Ding, A. J.: Multifunctional Products of Isoprene Oxidation in Polluted

563   Atmosphere and Their Contribution to SOA, Geophys. Res. Lett., 48(1), 1–10,

564   doi:10.1029/2020GL089276, 2021.

565 Yan, C., Nie, W., Äijälä, M., Rissanen, M. P., Canagaratna, M. R., Massoli, P., Junninen, H., Jokinen, T.,

566   Sarnela, N., Häme, S. A. K., Schobesberger, S., Canonaco, F., Yao, L., Prévôt, A. S. H., Petäjä, T.,

567   Kulmala, M., Sipilä, M., Worsnop, D. R. and Ehn, M.: Source characterization of highly oxidized

568   multifunctional compounds in a boreal forest environment using positive matrix factorization, Atmos.

569   Chem. Phys., 16, 12715–12731, doi:10.5194/acp-16-12715-2016, 2016.

570 Yan, C., Yin, R., Lu, Y., Dada, L., Yang, D., Fu, Y., Kontkanen, J., Deng, C., Garmash, O., Ruan, J.,

571   Baalbaki, R., Schervish, M., Cai, R., Bloss, M., Chan, T., Chen, T., Chen, Q., Chen, X., Chen, Y.,

572   Chu, B., Dällenbach, K., Foreback, B., He, X., Heikkinen, L., Jokinen, T., Junninen, H.,

573   Kangasluoma, J., Kokkonen, T., Kurppa, M., Lehtipalo, K., Li, H., Li, H., Li, X., Liu, Y., Ma, Q.,

574   Paasonen, P., Rantala, P., Pileci, R. E., Rusanen, A., Sarnela, N., Simonen, P., Wang, S., Wang, W.,

575   Wang, Y., Xue, M., Yang, G., Yao, L., Zhou, Y., Kujansuu, J., Petäjä, T., Nie, W., Ma, Y., Ge, M.,

576   He, H., Donahue, N. M., Worsnop, D. R., Veli-Matti Kerminen, Wang, L., Liu, Y., Zheng, J.,

577   Kulmala, M., Jiang, J. and Bianchi, F.: The Synergistic Role of Sulfuric Acid, Bases, and Oxidized

578   Organics Governing New-Particle Formation in Beijing, Geophys. Res. Lett., 48, 2020GL091944,

579   doi:10.1029/2020gl091944, 2021.

580 Yao, L., Garmash, O., Bianchi, F., Zheng, J., Yan, C., Kontkanen, J., Junninen, H., Mazon, S. B., Ehn, M.,

581   Paasonen, P., Sipilä, M., Wang, M., Wang, X., Xiao, S., Chen, H., Lu, Y., Zhang, B., Wang, D., Fu,

582   Q., Geng, F., Li, L., Wang, H., Qiao, L., Yang, X., Chen, J., Kerminen, V.-M., Petäjä, T., Worsnop,

583   D. R., Kulmala, M. and Wang, L.: Atmospheric new particle formation from sulfuric acid and amines

584   in a Chinese megacity, Science (80-.)., 361, 278–281, doi:10.1126/science.aao4839, 2018.

585   Ye, C., Yuan, B., Lin, Y., Wang, Z., Hu, W., Li, T., Chen, W., Wu, C., Wang, C., Huang, S., Qi, J., Wang,

586   B., Wang, C., Song, W., Wang, X., Zheng, E., Krechmer, J. E., Ye, P., Zhang, Z., Wang, X., Worsnop,

587   D. R. and Shao, M.: Chemical characterization of oxygenated organic compounds in the gas phase

588   and particle phase using iodide CIMS with FIGAERO in urban air, Atmos. Chem. Phys., 21(11),

589   8455–8478, doi:10.5194/acp-21-8455-2021, 2021.

590   Yu, K., Zhu, Q., Du, K. and Huan, X. F.: Characterization of nighttime formation of particulate organic

591   nitrates based on high-resolution aerosol mass spectrometry in an urban atmosphere in China, Atmos.

592   Chem. Phys., 19(7), 5235–5249, doi:10.5194/acp-19-5235-2019, 2019.

593   Zhang, Y., Li, D., Ma, Y., Dubois, C., Wang, X., Perrier, S., Chen, H., Wang, H., Jing, S., Lu, Y., Lou,

594   S., Yan, C., Nie, W., Chen, J., Huang, C., George, C. and Riva, M.: Field Detection of Highly

595   Oxygenated Organic Molecules in Shanghai by Chemical Ionization–Orbitrap, Environ. Sci.

596   Technol., doi:10.1021/acs.est.1c08346, 2022.

597   Zhao, Y., Thornton, J. A. and Pye, H. O. T.: Quantitative constraints on autoxidation and dimer formation

598   from direct probing of monoterpene-derived peroxy radical chemistry, Proc. Natl. Acad. Sci. U. S.

599   A., 115(48), 12142–12147, doi:10.1073/pnas.1812147115, 2018.

600

Table 1 Summary of the four cases including the meteorological conditions and concentrations of trace gases and 2N-OOMs

Case	Time	$\overline{PM_{2.5}}$ (μg m^{-3})	$\overline{Solar}$ (W m^{-2})	$\bar{T}$ (°C)	$\overline{RH}$ (%)	$\overline{[O_3]}$ (ppb)	$\overline{[NO]}$ (ppb)	$\overline{[NO_2]}$ (ppb)	$\overline{[NO_3]}$ (ppt)	$\overline{[2N-OOM_{Aro}]}$ ($\times 10^6$ cm^{-3})	$\overline{[2N-OOM_{Alu}]}$ ($\times 10^6$ cm^{-3})	$\overline{[2N-OOM_{MT}]}$ ($\times 10^6$ cm^{-3})	$\overline{[2N-OOM_{Total}]}$ ($\times 10^6$ cm^{-3})
CL$_{day}$	Nov. 4th 12:00 - 14:00	7.5	635.6	18.9	35.2	41.9	3.2	8.2	0.1	6.3	11.7	2.3	20.8
CL$_{night}$	Nov. 4th 23:00 - Nov. 5th 01:00	9.5	2.4	13.0	64.1	8.0	2.9	40.5	0.2	1.3	6.0	2.3	9.8
PL$_{day}$	Nov. 7th 12:00 - 14:00	44.0	384.5	23.9	30.5	73.9	2.2	20.6	0.3	6.4	23.8	4.3	36.2
PL$_{night}$	Nov. 7th 23:00 - Nov. 8th 01:00	60.5	2.5	17.8	44.9	27.2	2.1	38.7	6.2	3.1	17.4	5.3	26.5

Figure Captions

Figure 1. (a) Average mass spectrum of the detected OOMs during the whole campaign. The pie chart shows the fractions of OOMs with different number of nitrogen and carbon atoms; (b) The fractions of 0N-OOMs, 1N-OOMs, 2N-OOMs and 3N-OOMs among total OOMs as a function of carbon number (nC).

Figure 2. The timeseries of 2N-OOMs originated from different precursors. Four sub-periods were selected to further investigate the fractional distribution of different type of OOM molecules as shown in the pie chart, including a clean daytime case (12:00 to 14:00 on November 4th, $PM_{2.5}$=7.5 μg m^{-3}, CL_{day}), a clean nighttime case (23:00 on November 4th to 01:00 on November 5th, $PM_{2.5}$=9.5 μg m^{-3}, CL_{night}), a daytime case in a PM episode (12:00 to 14:00 on November 7th, $PM_{2.5}$=44.0 μg m^{-3}, PL_{day}) and a nighttime case in a PM episode (23:00 on November 7th to 01:00 on November 8th, $PM_{2.5}$=60.5 μg m^{-3}, PL_{night}). The sizes of pie charts are scaled to the total concentrations of 2N-OOMs.

Figure 3. The fractions of 2N-OOM$_{Ali}$ with different carbon numbers in the four cases.

Figure 4. (a) Statistical distribution of the correlation coeffients (Spearman type) between 2N-OOMs and solar radiation ($R_{2N-OOMs - solar}$) in red and the correlation coeffients between 2N-OOMs and [NO$_3$] ($R_{2N-OOMs - NO3}$) in blue for 2N-OOMs from different precursors. The horizontal lines are the median values, boxes denote the 25th- and 75th- percentile values, and whiskers represent the 10th- and 90th- percentile values. (b) The diel patterns of 2N-OOMs from different precursors.

Figure 5. Scatter plot of $R_{2N-OOMs - NO3}$ against $R_{2N-OOMs - solar}$ for specific 2N-OOM species.

Figure 6. The nO$_{eff}$ of 2N-OOMs derived from different precursors in the four cases, the error bars represent the standard deviations.

Figure 7. Effective oxygen number (nO$_{eff}$) of 2N-OOMs as a function of (a) NO concentration and (b) NO$_x$ concentration. The colored squares represent the real measurements. The filled markers indicate the median values in the range as horizontal error bars show, the vertical error bars denote the 25th- and 75th-percentile values.
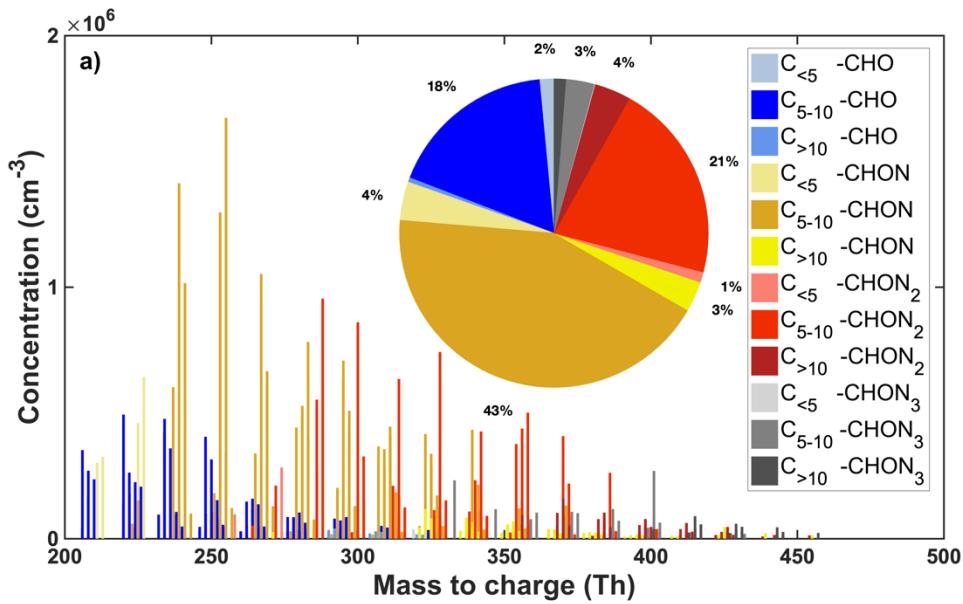
Figure 1a
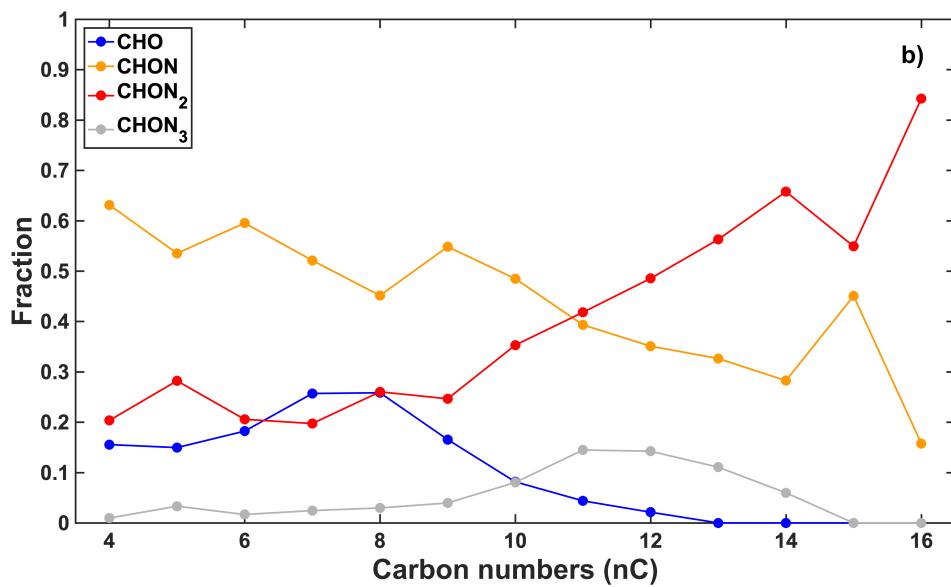
Figure 1b
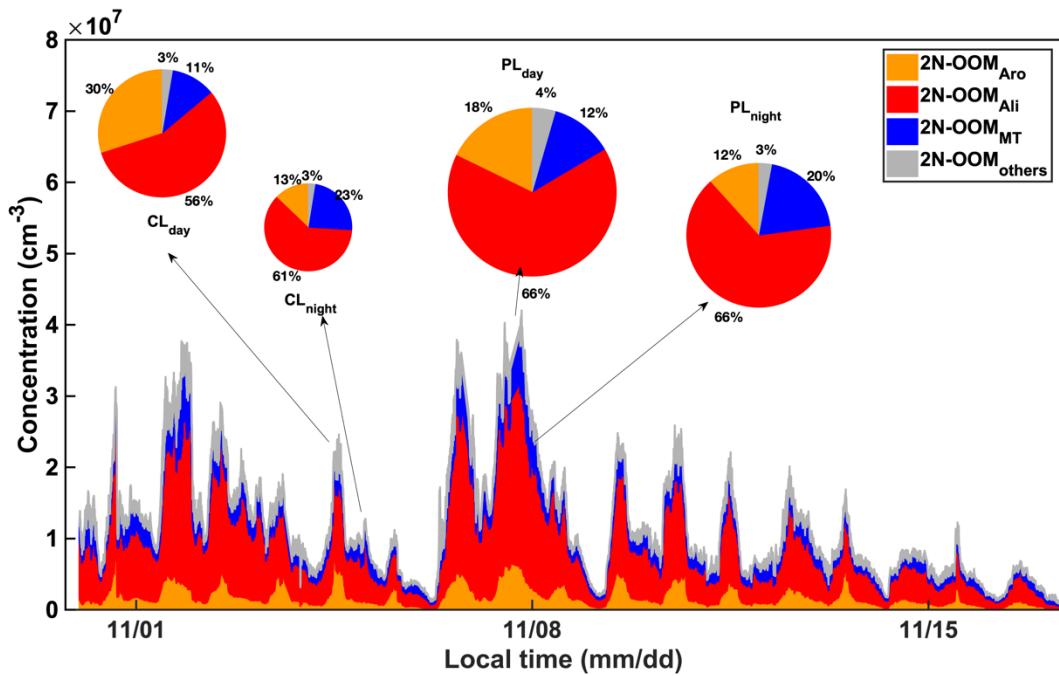
Figure 2
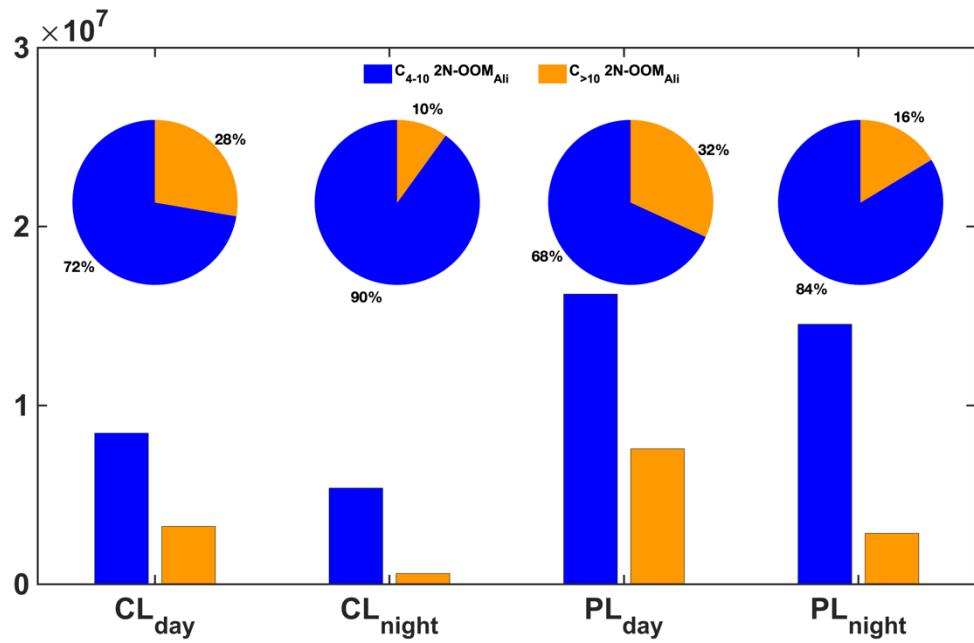
Figure 3
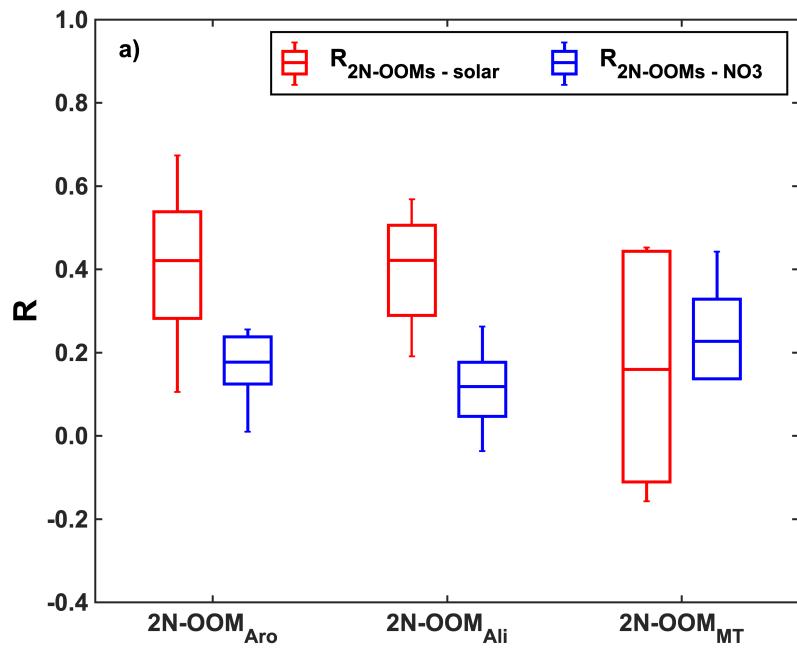
Figure 4a
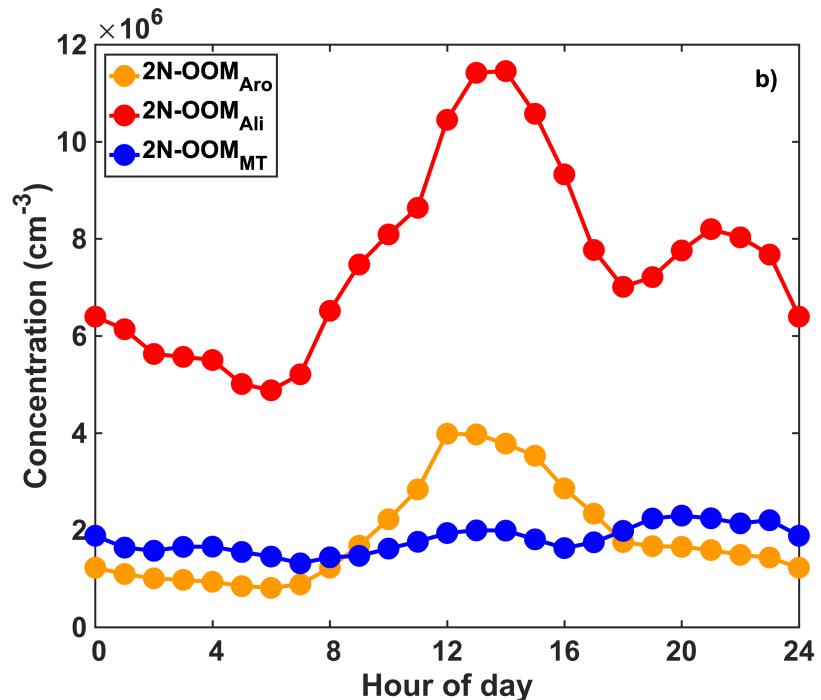
Figure 4b
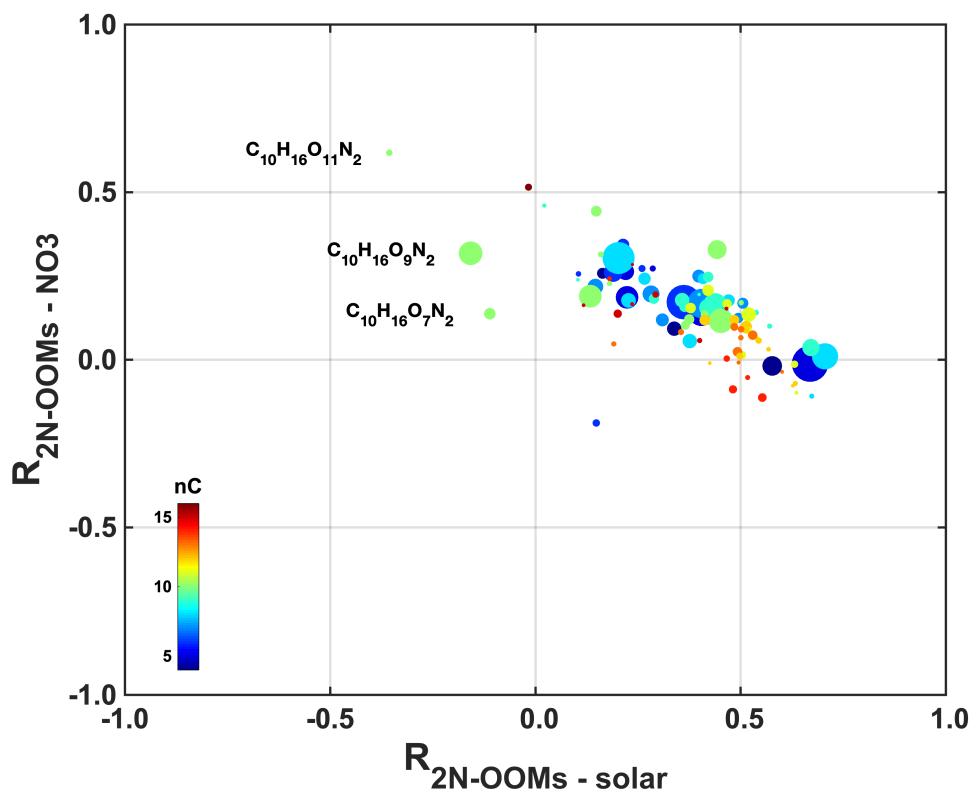
Figure 5
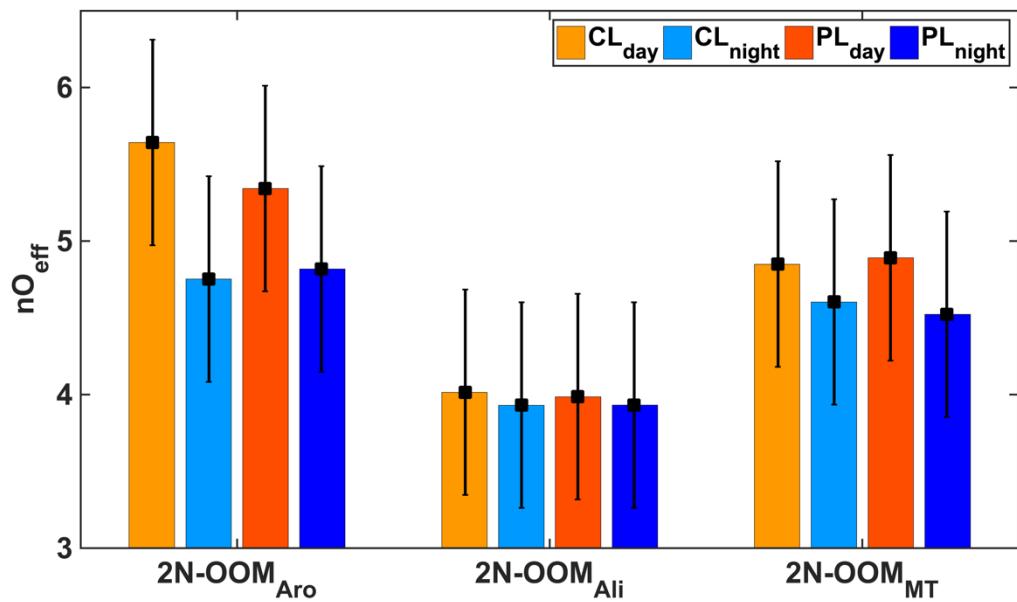
Figure 6

Figure 7a

Figure 7b